Mechanical and optical properties of MgAl2O4 ceramics and ballistic efficiency of spinel based armour

Caroline Gajdowski, Raffaele d'Elia, Norbert Faderl, Judith Böhmler, Yannick Lorgouilloux, Sébastien Lemonnier, Anne Leriche

▶ **To cite this version:**

Caroline Gajdowski, Raffaele d'Elia, Norbert Faderl, Judith Böhmler, Yannick Lorgouilloux, et al.. Mechanical and optical properties of MgAl2O4 ceramics and ballistic efficiency of spinel based armour. Ceramics International, 2022, 48 (13), pp.18199-18211. 10.1016/j.ceramint.2022.03.079 . hal-03850557

HAL Id: hal-03850557
https://hal.science/hal-03850557v1

Submitted on 26 Nov 2024

HAL is a multi-disciplinary open access archive for the deposit and dissemination of scientific research documents, whether they are published or not. The documents may come from teaching and research institutions in France or abroad, or from public or private research centers.

L'archive ouverte pluridisciplinaire **HAL**, est destinée au dépôt et à la diffusion de documents scientifiques de niveau recherche, publiés ou non, émanant des établissements d'enseignement et de recherche français ou étrangers, des laboratoires publics ou privés.

Mechanical and optical properties of $MgAl_2O_4$ ceramics and ballistic efficiency of spinel based armour

Caroline Gajdowski [a,b,*], Raffaele D'Elia [a], Norbert Faderl [a], Judith Böhmler [a,**], Yannick Lorgouilloux [b], Sébastien Lemonnier [a], Anne Leriche [b]

[a] Institut Franco-allemand de Recherches de Saint-Louis, 5 Rue du Général Cassagnou, 68301, Saint-Louis Cedex, France

[b] Univ. Polytechnique Hauts-de-France, INSA Hauts-de-France, CERAMATHS – Laboratoire de Matériaux Céramiques et de Mathématiques, F-59313 Valenciennes, France

A B S T R A C T

This study was devoted to the understanding of the influence of $MgAl_2O_4$ ceramic properties on their ballistic performances. By modifying the processing parameters, ceramics with different microstructures were obtained. Among them, a transparent $MgAl_2O_4$ spinel with an in-line transmission between 77% and 83% in the visible range, an average grain size of 8.6 μm and good mechanical properties (11.3 GPa in Knoop hardness and 2.5 MPa$\sqrt{m}$ in fracture toughness) was produced. A thorough characterisation of the ceramics was accomplished in order to establish a link between microstructure, mechanical properties and ballistic protective performances against an armour piercing projectile of calibre 7.62x51 mm. The ballistic evaluation demonstrated the advantage of using a spinel layer as the strike face to stop a threat, while reducing drastically the thickness and the areal density of the transparent multilayer, compared to a simple glass armour. $MgAl_2O_4$ spinel with fine grains presented a better combination of mechanical properties compared to coarser microstructures, hence a better potential to damage a projectile at the impact.

Keywords:
Spinel
MgAl2O4
Transparent
Armour
Sintering
Ballistic performance
Mechanical properties

1. Introduction

Transparent ceramics have been the focus of many studies in the past few years due to their high potential, notably in military applications, such as armours, optical lenses and lasers sources [1–5]. The improvement of transparent ballistic protections has particularly been investigated [6–8]. Indeed, bulletproof windows or helmet visors are generally an assembly of glass and polymer layers. However, the high thickness necessary to withstand projectile perforation induces voluminous and heavy systems, thus more difficult to carry. The approach of enhancement is to use a hard transparent ceramic as the front layer of the armour: at the impact, the projectile tip will be eroded, fragmented and slowed down by the hard layer. Thus, a thinner glass thickness is needed, diminishing the total volume and weight of the protection [1,4,6–11]. For this application, $MgAl_2O_4$ spinel, polycrystalline and single-crystal Al_2O_3 and AlON ($Al_{23}O_{27}N_5$) present the appropriate properties: high transparency in the visible and infrared ranges (>95% of the theoretical transmission of the material) and good mechanical properties (hardness, toughness and mechanical strength). The capacity of these ceramics to withstand shots was already highlighted in the literature [5,9,12,13]. In the work of Strassburger [10], multilayers with and without ceramic were tested against a 7.62 × 51 mm AP (Armor Piercing) projectile. An areal density (AD) of 160 kg/m^2 was necessary with the standard glass protection to avoid perforation, while by using a 2.2 mm thick spinel or AlON, it was possible to lighten the system to 70 kg/m^2. Krell et al. [9] applied a similar approach and showcased the high potential of $MgAl_2O_4$ ceramic for transparent armour: the areal density of the protection to avoid perforation was equal to 65 kg/m^2 when using spinel (2.2 mm thick), while an AD of 95 kg/m^2 was reached with a 2 mm-thick sapphire.

The use of $MgAl_2O_4$ spinel in ballistic applications is a good compromise, as its high theoretical in-line transmission is above 83% in the visible range and it presents a good combination of mechanical properties [4,8]. Moreover, in terms of processing, it requires a lower sintering temperature than alumina, sapphire and AlON. To obtain the required properties for ballistic protection, a fine control of the final

* Corresponding author. Institut franco-allemand de recherches de Saint-Louis, 5 rue du Général Cassagnou, 68301, Saint-Louis Cedex, France.
** Corresponding author.
E-mail addresses: caroline.gajdowski@bcrc.be (C. Gajdowski), judith.boehmler@isl.eu (J. Böhmler).

microstructure by means of a carefully chosen procedure is necessary to avoid defects and to limit grain growth. Indeed, the presence of pores or impurities will affect transparency and mechanical properties. Then, a fine grain size has to be favoured in order to obtain high mechanical characteristics, according to the Hall-Petch law [14–17].

The literature reports various approaches to develop transparent spinel. From the raw material point of view, commercial $MgAl_2O_4$ powders are commonly used [18–26]. Some articles report the synthesis of the spinel powder from chloride or nitride [27–29]. Reactive sintering between MgO and Al_2O_3 is also employed to obtain non or stoichiometric $MgAl_2O_4$ [30–33]. Concerning sintering techniques, Hot Press (HP) of $MgAl_2O_4$ is commonly used since pressure assisted method can provide higher driving force to eliminate pores and enhance densification [30,33–35]. For example, Gilde et al. [36] sintered commercial powder (S30CR, Baikowski) with 0.75wt% LiF by HP at 1650 °C for 3h (200 MPa) followed by HIP at 1900 °C for 6h. Good transmission was obtained (82% at 632 nm), however the microstructure presented coarse grains between 200 and 300 µm. The study of Zhu et al. [19] showed transparent spinel after the sintering of pure S30CR powder by HP at 1500 °C for 12h (20 MPa), preceded by a presintering of the samples at 1300 °C for 2h. Transmission of 40–75% in the visible range, 12.5 GPa in hardness and 1.2 MPa$\sqrt{m}$ in toughness were obtained. An average grain size equal to 1.8 µm was measured, however the microstructure revealed abnormal grain growth and pores.

Spark Plasma Sintering (SPS) is usually employed to obtain spinel with high transmission and fine microstructure at low temperature [16,17,20,21,23,37,38]. Nanometric grains of 250 nm, transmission of 74% at 500 nm and hardness of 16 GPa (HV3) can be observed after SPS at 1300 °C of a fine commercial powder (S30CR) [23]. Even finer microstructure was reported by Sokol et al. [16], where a dense spinel with 50 nm grains was obtained after High Pressure SPS at 1000 °C with a load of 1000 MPa. The transmission values were between 65 and 80% in the visible range and the hardness was equal to 18.5 GPa (HV1).

A common issue reported during SPS and HP processes of transparent oxide ceramics is the coloration of the sample. The observation of blackening or translucency can be caused by a contamination from the graphite tools and the presence of oxygen vacancies generated under vacuum [21,39–41]. The addition of LiF has shown a beneficial effect to counter graphite pollution of $MgAl_2O_4$ and other transparent ceramics. Several studies also demonstrated a better homogeneity of the microstructure, an improvement of the optical quality and lower sintering temperatures when LiF is added [30,31,34,42–44]. Nevertheless, an improper quantity or mix, or an incomplete elimination of the sintering aid may induce grain growth, porosity or secondary phases formation in the ceramic [30,42,43,45,46].

To avoid graphite tools, Pressureless Sintering (PS) can be applied. Green body has firstly to be prepared, either by dry compaction (uniaxial and cold isostatic pressing) [20,42,47,48] or by wet methods (slip-, gel-, or tape-casting) [21,22,32,49]. Then, the green bodies can be sintered in air or in vacuum without applying pressure [20,22,42,47,48]. However, a post-treatment by Hot Isostatic Pressing (HIP) is generally required in order to eliminate residual porosity and then, to obtain transparent ceramics. After PS at 1550 °C of a commercial powder (S30CR, Baikowski), Maca et al. [20] obtained a spinel sample with 94.9% in relative density. By applying a HIP step at 1500 °C for 1h under argon (200 MPa), the density increased to 99.9% and, even if it remains low due to the presence of remaining pores, the in-line transmission was improved to 60% (632 nm). From the microstructural point of view, the final grain size was fine with an average equal to 1 µm. A value of 13 GPa of Vickers hardness (HV1) was indicated. The ceramic made by Liu et al. [48] by PS (1525 °C for 3h) followed by HIP (1600 °C for 3h) using the same commercial powder from Baikowski with 0.1 wt% CaO as sintering aid presented fine grains as well (1.5 µm), a high line-transmission of 82.5% at 600 nm and similar hardness (13.2 GPa). The better optical result could be explained by the use of CaO and the higher temperatures and times during the HIP treatment.

As seen from the literature, the possibilities to develop transparent $MgAl_2O_4$ are considerable and diversified. Although a majority of papers deal with the fabrication and the characterisation of spinel, the link between optical quality, grain size, mechanical properties and ballistic performances has been barely reported. The paper of McCauley and Patel [50] is one of the few articles dealing with the comparison of two references of $MgAl_2O_4$ spinel with different grain size (0.6 and 1.6 µm), including a thorough characterisation in terms of microstructure, mechanical properties (hardness, fracture toughness, spherical indentation, quasi-static bend bar strength, dynamic compressive strength) and ballistic tests (impact depth into an aluminium backing and distribution of the fragment sizes with an AP 7.62 × 51 mm projectile). Their results indicated few influences of the grain size on some mechanical aspects (bending strength, Weibull modulus, fracture toughness), however their data suggested a better resistance to penetration with a fine microstructure than a larger grain ceramic.

In a previous work, Gajdowski et al. [51] prepared $MgAl_2O_4$ ceramics by using high purity powder, as well as a pressureless sintering approach to prevent contamination by graphite tools, grain growth and potential secondary phases. The application of a HIP treatment was found to be necessary and its processing conditions strongly influenced the final properties of the ceramics. Nonetheless, this work only focused on the relationship between sintering parameters, microstructural properties and optical quality. Fully dense ceramics with high transparency in the visible and IR ranges were developed with coarse and heterogeneous grain size distributions. This study follows on from this previous work and aims to characterize the ballistic performance of these ceramics in relation to their mechanical and microstructural properties. Spinel ceramics were developed following the same procedure: pressureless sintering with a post-treatment by hot isostatic pressing. In order to correlate the microstructural properties to optical, mechanical and ballistic results, samples with different final microstructures were achieved by varying the process parameters. This work allowed to highlight the impact of the microstructure on the mechanical properties of the final ceramic material, hence the ballistic efficiency.

2. Experimental procedure

2.1. Fabrication of the ceramics

$MgAl_2O_4$ ceramics were prepared with a spinel powder referenced S25CRX from Baikowski (France). The supplier indicated a grain size d_{50} of 0.43 µm, a specific surface area equal to 17 m^2/g and a low level of impurities (50 ppm in total). The raw powder was dry compacted by uniaxial compaction, then followed by cold isostatic pressing. The obtained green bodies were subsequently pressureless sintered in a vacuum furnace (Lilliput, ECM Technology) without sintering additive. A post-treatment by hot isostatic pressing (EPSI Inc.) under Argon pressure

Table 1
Pressureless sintering and HIP conditions of the $MgAl_2O_4$ ceramics characterised in this paper.

$MgAl_2O_4$ ceramic	A	B	C	D	E
Pressureless sintering (°C/h)	1500/2	1500/2	1500/2	1500/24	Commercial PERLUCOR AA
Hot isostatic pressing (°C/h)	–	1800/1	1800/10	1600/10	

(200 MPa) was applied to eliminate residual porosity, followed by an annealing treatment in air. This procedure is already described in a previous work [51]. A selection of four spinel ceramics obtained in different conditions of sintering and HIP was processed. Sample labelled A was simply pressureless sintered. In addition to changing some sintering parameters, samples labelled B, C and D were subsequently treated by HIP using different temperatures and holding times (Table 1). For comparison, a commercial spinel, PERLUCOR grade AA from CeramTec (Germany), was selected and referenced as sample E.

2.2. Methods of characterisation

Sintered samples of 21.0 ± 0.6 mm in diameter and 2.0 ± 0.1 mm thick were prepared for the different characterisation tests, whereas larger samples, 60.0 ± 0.5 mm in diameter and 4.0 ± 0.3 mm in thickness, were prepared for the ballistic tests. The latter were fully analysed and no influence of the scale up was observed on the ceramic final properties in terms of microstructure, in-line transmission and Knoop hardness.

2.2.1. Relative density

The theoretical bulk density of spinel $MgAl_2O_4$ is equal to 3.58 g/cm^3. To determine the relative density, the ceramics were weighted three times in air, in distilled water and then wet (Archimedes method). An average value was calculated for each grade.

2.2.2. Optical properties

After annealing and mirror-polishing the ceramics, the In-Line Transmission (ILT) was measured between 300 and 3000 nm with a UV-VIS-IR spectrophotometer (Cary 7000 UMS, Agilent Technologies) with a scan rate equal to 600 nm/min.

2.2.3. Microstructure

Microstructure analyses were undertaken by Scanning Electron Microscopy (SEM) with a Nova NanoSEM 450 (FEI Company) after a mirror-like polishing step. For the determination of the mean grain size, a minimum of five images were used, in which no less than three hundred grains were measured with the software ImageJ, then their sizes were arithmetically averaged.

2.2.4. Mechanical properties

- *Hardness*

Knoop hardness was analysed with a micro-indenter from Buehler. As hardness strongly depends on the loading due to the Indentation Size Effect (ISE) [52], loads between 0.05 and 2 kg (0.49 and 19.6 N) were applied. The Multi-Fractal Scaling Law (MFSL) was used in this analysis to estimate a load-independent hardness value for each sample [53], following this equation (Eq. (1)):

$$HK\,(MFSL) = HK\,\infty\,(1 + L^*/L)^{0.5} \quad \text{Eq. 1}$$

With $HK\infty$ the load-independent Knoop hardness, L^* the critical length of the material indicating the transition between behaviours (from size-dependent to size-independent) and L the length of the indent long diagonal.

- *Elastic modulus*

Elastic modulus E was obtained from the measurements of transversal and longitudinal waves velocities V_T and V_L with the aid of an ultrasonic thickness gage (Olympus 45 MG). From these values, the Poisson coefficient ν can be calculated (Eq. (2)), then the modulus can be determined (Eq. (3)):

$$\nu = (1–2 \times (V_T/V_L)^2) / (2–2 \times (V_T/V_L)^2) \quad \text{Eq. 2}$$

$$E = (V_L^2 \times \rho \times (1 + \nu) \times (1–2\,\nu)) / ((1 – \nu) \times 10^9) \quad \text{Eq. 3}$$

With ρ the bulk density (kg/m^3) of the sample.

The average elastic modulus was estimated on ten samples of each sintered grade and on twenty samples for the commercial ceramic.

- *Fracture toughness*

Cracks generated during Vickers indentations were analysed to determine the fracture toughness on the basis of the model of Niihara [54]. The load had to be adapted for each grade of spinel depending on the apparition of cracks. A minimum of ten indentations were made for the estimation of K_{1C}. A distinction was made between Palmqvist and median cracks according to the ratio c/a (c and a representing respectively the cracks length and the diagonal of the indentation). When the sample showed Palmqvist cracks with $0.25 \leq c/a \leq 2.5$, Eq. (4) was used, whereas K_{1C} was calculated according to Eq. (5) when the ratio c/a was superior to 2.5 for median cracks.

$$K_{1C} = 0.035 \times (c/a)^{-0.5} \times (H/(E \times \Phi))^{-2/5} \times ((H \times a^{0.5})/\Phi) \quad \text{Eq. 4}$$

$$K_{1C} = 0.129 \times (c/a)^{-3/2} \times (H/(E \times \Phi))^{-2/5} \times ((H \times a^{0.5})/\Phi) \quad \text{Eq. 5}$$

With Φ a factor considered equal to 3, H the Vickers hardness and E the Young modulus.

- *Flexural strength*

The characterisation of the equibiaxial flexural strength of the ceramics was done with the so-called Ball-on-3-Balls test (B3B) method. Introduced by Godfrey and developed by Börger et al. [55,56], B3B test determines the biaxial resistance in flexion of brittle samples such as ceramics. The B3B setup has been developed and mounted on a quasi-static press (Instron 5500-K9400) with a 5 kN load cell. The test was performed under quasi-static conditions (testing speed of 0.5 mm/min) up to the failure force. A specific setting was used, where the ceramic in the shape of a disc was positioned on one ball and three balls were placed on top of it (balls with a diameter of 15 mm). B3B tests were carried out on ten samples for each grade of fabricated spinel and more than twenty for the commercial ceramic. This is lower than the thirty samples normally required to take into account the statistical variability of the results but it already allows to identify trends. By estimating a failure stress σ_c and a probability of failure P_F for each sample of each grade of spinel, a 2 parameters-Weibull distribution was obtained. Then linearization was applied, leading to the equation Eq. (6):

$$\ln \ln (1 / (1 – P_F)) = (m \times \ln \sigma_c) – (m \times \ln \sigma_0) \quad \text{Eq. 6}$$

By applying the maximum likelihood method, the average failure stress σ_{av} and its standard deviation σ_{st} are obtained (Eq. (7) and Eq. (8)):

$$\sigma_{av} = \sigma_0 \times \Gamma \times (1 + 1/m) \quad \text{Eq. 7}$$

$$\sigma_{st} = \sigma_0 \times \sqrt{((\Gamma \times (1 + 2/m) – \Gamma^2 \times (1 + 1/m))} \quad \text{Eq. 8}$$

With $\Gamma\,(1 + x) \cong 1 – (3/4)^2 x + (3/4)x^2$

An observation by SEM of the fracture surfaces after the B3B tests was made for each grade of spinel in order to identify the fracture mode (transgranular or intergranular).

2.2.5. Ballistic performance

To characterize the ballistic performance of the ceramics, a similar approach to the work of Strassburger was used [10]. In his work, $MgAl_2O_4$ spinel from IKTS (Germany) were tested on an assembly made of one to three layers of glass and one layer of polycarbonate (4 mm thick). An AP projectile 7.62 × 51 mm was shot at a velocity of 850 ± 15 m/s. In this present paper, each grade of spinel was tested as the front face of a transparent multilayer made of soda lime glass sheets (150 ×

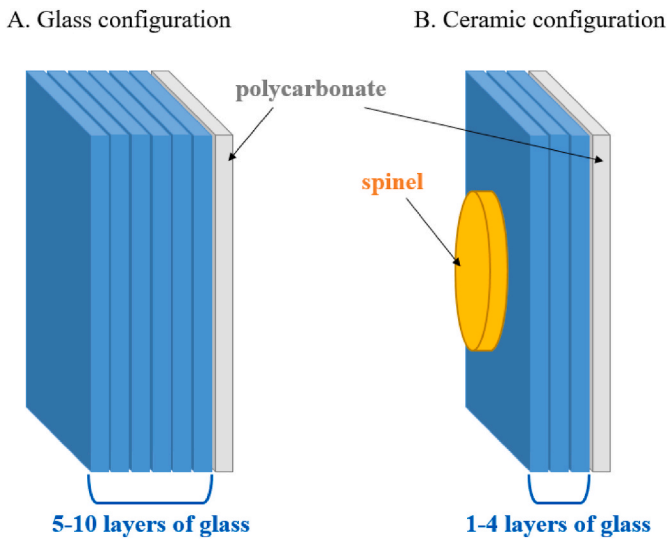

Fig. 1. Schematic of the assembly used for the ballistic test: (A) glass configuration and (B) ceramic configuration with a spinel layer as the strike face.

150 mm^2) and a polycarbonate layer (150 x 150 × 4 mm) put on the rear as the backing. Their bulk densities were equal to 2.44 g/cm^3 and 1.18 g/cm^3 respectively. A metallic frame kept the whole assembly tight without using glue. Fig. 1 shows a schematic of the multilayers evaluated in this study with the two configurations.

Table 2 reports the configuration of all the ballistic tests: the number of glass layers and their thicknesses, the total thickness and areal density of the multilayer, and the initial and residual velocities of the projectile. For each grade of spinel, four to five samples were processed and tested. The configuration of the multilayer, as well as the areal density (AD) of the armour, were modified for each shot. The glass thickness was increased progressively, while maintaining the thickness of the polycarbonate and the spinel to 4 mm. By increasing the glass thickness, and thus the areal density, the residual velocity decreased after perforation.

In order to highlight the advantage of the spinel layer to lower the global thickness and the areal density of a ballistic protection, a reference configuration without ceramic was also tested, labelled *glass*. For all of the configurations, with and without a ceramic layer, one shot was especially made on an assembly with a glass layer thick enough to avoid complete perforation. An armour piercing projectile with steel core of calibre 7.62 × 51 mm (P80) was used with an initial velocity of 820 ± 10 m/s. A triple exposure X-Ray system was used to estimate the residual velocity V_r of the projectile after perforation by taking three pictures at a known time interval. A high-speed camera was installed to visualize the impact from the back of the armour.

3. Results

3.1. Relative density

Measurements of the relative densities reported in Table 3 indicated a result equal to 96.9% for sample A and superior to 99.9% for the three other fabricated ceramics. The lower density of sample A resulted from residual pores, which were not eliminated during sintering. The application of a post-treatment by HIP led to the removal of these defects, thus to an increase of the density (samples B, C and D). In the case of the commercial spinel E, a relative density of 99.9% was measured.

3.2. Optical properties

In-line transmissions of the ceramics are shown in Fig. 2. The pressureless sintered ceramic A was characterised by a transmission close to zero on a wide range of wavelengths and started to slightly increase at 2000 nm to reach 5.5% at 3000 nm. As presented in the photo in Fig. 2, sample A was completely opaque after sintering. In the case of ceramics B, C and D, very high in-line transmission values were observed in the range of 77–86% between 400 and 800 nm and a minimum of 86% at 3000 nm. The combination of vacuum sintering and HIP proved to be a suitable process to obtain transparent ceramics with optical quality close to the commercial sample. This latter (sample E) showed the highest in-

Table 2
Number and thickness of glass layers, total thickness and total areal density of the multilayer, initial and residual velocities of the projectile for each test and each configuration. A positive outcome is indicated with "no" (*i.e.* no perforation), while a negative outcome (*i.e.* perforation) is indicated with "yes".

Configuration	# test	Number and thickness of glass layers	Total thickness (mm)	Total AD (kg/m^2)	Initial velocity (m/s)	Residual velocity (m/s)	Perforation yes/no
Glass	1	5 × 6 mm	34	77.9	831	383	yes
	2	7 × 6 mm	46	107.2	830	226	yes
	3	8 × 6 mm	52	121.8	805	86	yes
	4	9 × 6 mm + 1 × 2 mm	60	141.4	828	0	no
Spinel A	1	1 × 6 mm	14.1	34	816	538	yes
	2	2 × 6 mm	20.1	48.7	828	296	yes
	3	1 × 2 mm + 2 × 6 mm	22.1	53.6	819	263	yes
	4	1 × 3 mm + 3 × 6 mm	29.1	70.6	815	0	no
Spinel B	1	1 × 6 mm	14.2	34.3	835	499	yes
	2	2 × 6 mm	20	48.3	830	261	yes
	3	1 × 3 mm + 2 × 6 mm	23.5	57.4	811	203	yes
	4	4 × 6 mm	32.1	78	827	0	no
Spinel C	1	1 × 6 mm	14.1	34	814	506	yes
	2	2 × 6 mm	19.9	48	827	270	yes
	3	1 × 3 mm + 1 × 6 mm	23	55.6	810	142	yes
	4	1 × 3 mm + 1 × 6 mm	23.1	56	825	242	yes
	5	1 × 3 mm + 3 × 6 mm	29.1	70.6	837	0	no
Spinel D	1	1 × 6 mm	14.1	34	820	497	yes
	2	2 × 6 mm	20.1	48.7	815	197	yes
	3	1 × 3 mm + 2 × 6 mm	22.9	55.3	823	161	yes
	4	1 × 3 mm + 2 × 6 mm	23.4	57.1	807	87	yes
	5	3 × 6 mm	26.4	64.4	818	0	no
Spinel E	1	1 × 6 mm	14	33.7	828	576	yes
	2	2 × 6 mm	20	48.3	823	292	yes
	3	1 × 2 mm + 2 × 6 mm	22	53.2	806	178	yes
	4	1 × 3 mm + 2 × 6 mm	23	55.6	822	177	yes
	5	3 × 6 mm	26	63	811	0	no

Table 3
Relative densities, in-line transmissions (λ: 400-800 nm) and mean grain sizes of the $MgAl_2O_4$ ceramics.

$MgAl_2O_4$ ceramic	A	B	C	D	E
Relative density (%)	96.9	>99.9	>99.9	>99.9	>99.9
In-line transmission (%)	0	78–84	81–86	77–83	83–86
Mean grain size (μm)	1.3	36.3	73.4	8.6	10.2
Range of grain sizes (μm)	0.4–2.9	6.2–310	7.2–510	2.7–22.4	1.1–48.5

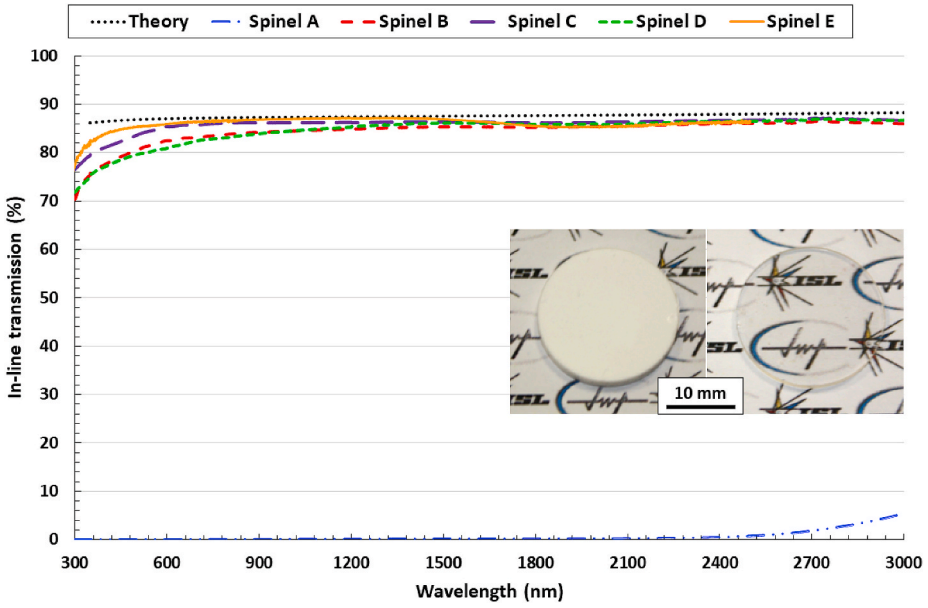

Fig. 2. In-line transmission curves of the $MgAl_2O_4$ ceramics. The inserted photos show one opaque and one transparent ceramics synthetized in this paper (samples A and B respectively). (For interpretation of the references to color in this figure legend, the reader is referred to the Web version of this article.)

line transmission in the visible domain, between 83 and 86%, and close to the theory in the infrared. Experimental values of ILT at 400 and 800 nm are reported in Table 3.

3.3. Microstructure

SEM observations of the polished surfaces presented in Fig. 3 revealed different microstructures between manufactured and commercial ceramics. Sample A presented a porous microstructure, as expected from the relative density and the optical quality. The grain size distribution was homogeneous and showed a fine average size with 1.3 μm. Numerous pores with size ranging from 50 to 400 nm were localized at grain boundaries and in the grains. Intragranular pores are generally detrimental since they are difficult to eliminate, and cause translucency or opacity. In this study, these defects were successfully removed during HIP, as samples B, C and D showed poreless microstructures. However, the full densification occurring during post-treatment was generally accompanied by grain growth. After HIP treatment at 1800 °C for 1h, sample B exhibited abnormal grain growth with isolated and large grains up to 310 μm. By increasing the holding time of post-treatment to 10h, more general exaggerated grain growth was observed for sample C with grains reaching 510 μm. In the case of sample D processed at a lower HIP temperature, a homogeneous but dispersed grain size distribution was obtained. In addition, the latter sample presented the finest and poreless microstructure with a mean value equal to 8.6 μm. Finally, SEM observations of the commercial spinel E revealed a microstructure with two distinct populations of grains for a mean grain size equal to 10.2 μm. The average values and the range of grains size obtained for each spinel are reported in Table 3.

3.4. Mechanical properties

- *Hardness*

The evolution of the Knoop hardness of the five ceramics is represented Fig. 4 as function of the applied load. At the lowest load (0.49 N), the hardness reached values between 15 and 16 GPa, which corresponded respectively to sample A and sample E. When increasing the load to 19.6 N, hardness values diminished to 11–12.2 GPa. Globally, among the sintered ceramics, sample A presented the lowest values, whereas sample D showed the highest. Interestingly, the commercial spinel displayed close hardness to the sintered ceramic D.

By using the multifractal scaling law (Eq. (1)), it is possible to obtain the load-independent Knoop hardness HK_∞ (reported in Table 4), useful to compare samples with different microstructures. The results were very close, however some tendencies have been observed: the porous sample A showed the lowest value with 10.3 GPa. By applying HIP during the process, the hardness increased, as indicated by samples B, C and D with 11, 10.9 and 11.3 GPa respectively. For the commercial spinel E, the load-independent hardness was equal to 11.2 GPa. These values are consistent with the common hardness values reported in the literature for $MgAl_2O_4$ in the range 11–15 GPa, depending on the applied load and grain size. Knoop hardness HK_2 of 12.1 GPa was indicated [52], and between 11 and 11.5 GPa for loads above 10 N [57].

- *Elastic modulus*

Mean values of the elastic modulus E of each $MgAl_2O_4$ ceramic are reported in Table 4. The Poisson coefficients estimated from Eq. (2) fluctuated between 0.25 and 0.28 for the fabricated samples. In the case

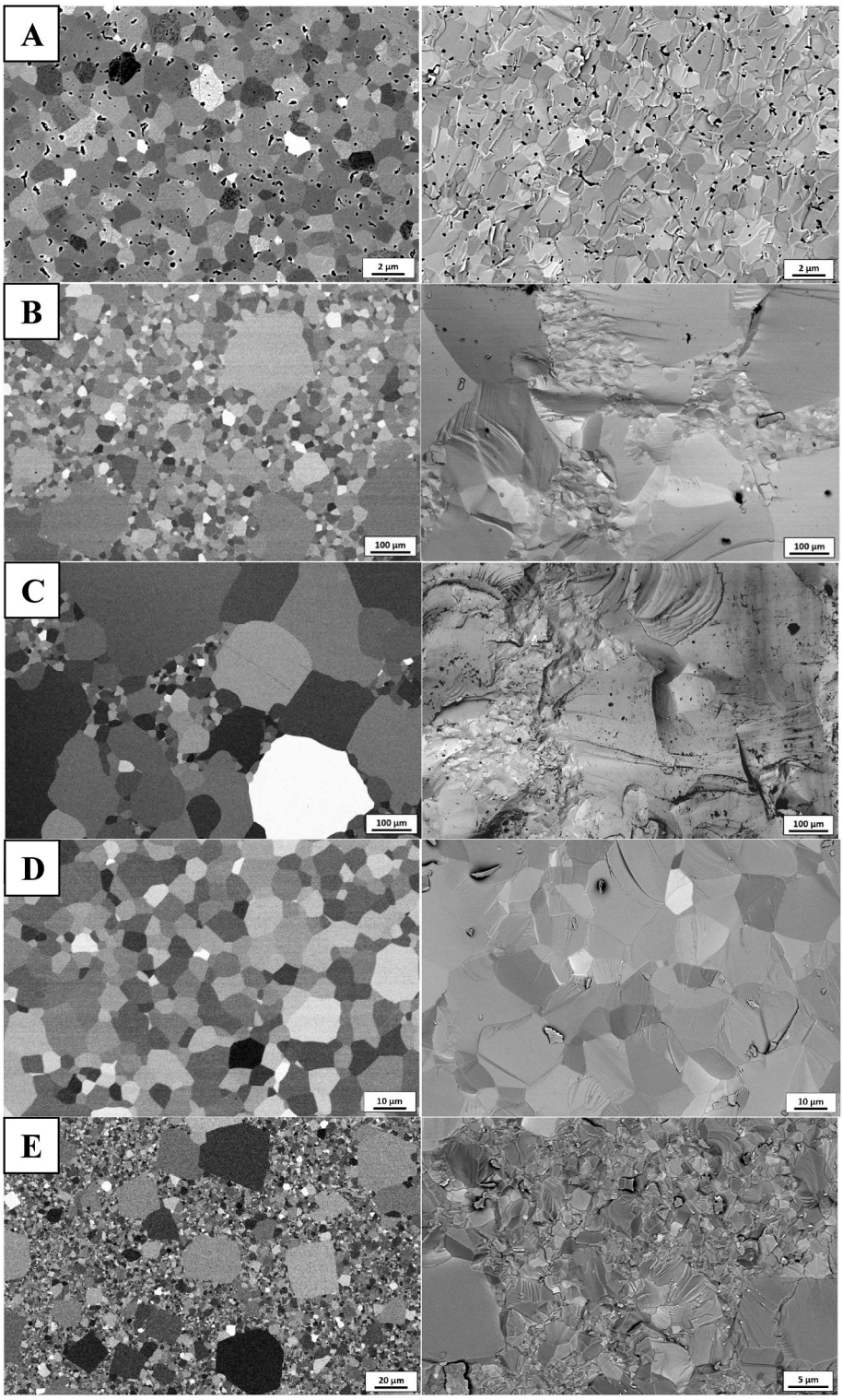

Fig. 3. SEM images of the $MgAl_2O_4$ ceramics: polished surface (left) and fracture after B3B tests (right).

of the commercial spinel, a value equal to 0.27 was obtained. For the elastic modulus, samples A, B and C can be compared first, as they were pressureless sintered in the same conditions. As shown in Table 4, their values of *E* moduli were very similar. As it can be noticed, the application of a HIP treatment did not substantially improve the modulus. Indeed, samples B and C showed a slight improvement or reduction respectively for this property compared to the ceramic A (266 GPa). The result for sample D was identical to the porous sample A. Finally, the commercial sample E showed the highest modulus with 279 GPa. These values were found to be similar to other studies on $MgAl_2O_4$ with results around 260–280 GPa [52,58–60].

- *Fracture toughness*

After Vickers indentations, cracks and indentations were measured in order to evaluate the parameters of the equation used for the

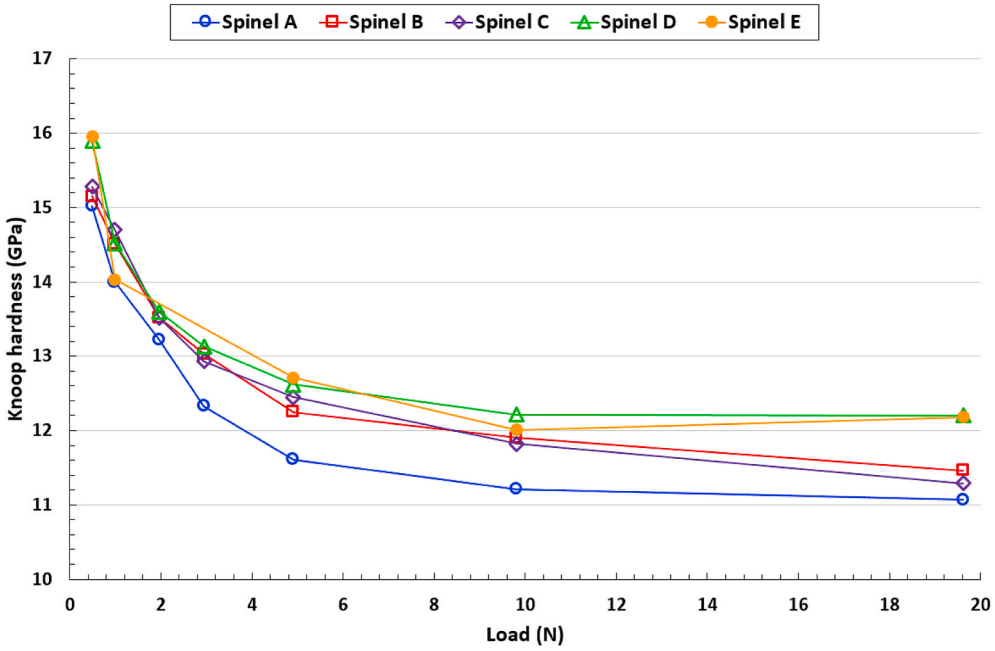

Fig. 4. Evolution of the Knoop hardness as function of the load . (For interpretation of the references to color in this figure legend, the reader is referred to the Web version of this article.)

Table 4
Summary of the mechanical properties of the $MgAl_2O_4$ ceramics.

$MgAl_2O_4$ ceramic	A	B	C	D	E
Knoop hardness MFSL (GPa)	10.3	11	10.9	11.3	11.2
Elastic modulus (GPa)	266 ± 6	286 ± 4	257 ± 4	267 ± 4	279 ± 1
Fracture toughness (MPa$\sqrt{m}$)	2.6 ± 0.5	1.6 ± 0.1	1.8 ± 0.3	2.5 ± 0.4	1.9 ± 0.2
Weibull modulus	5.6	5.3	4.3	6.8	7.2
Failure stress B3B (MPa)	253 ± 57	170 ± 40	194 ± 58	242 ± 43	556 ± 93

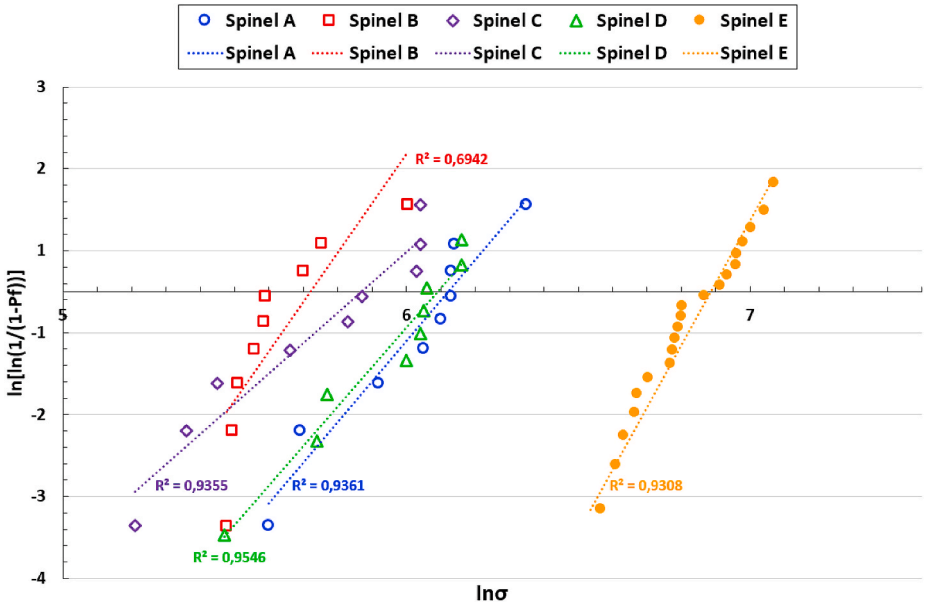

Fig. 5. 2-parameters Weibull distributions of the $MgAl_2O_4$ ceramics obtained from the B3B tests. Each symbol show one tested sample, the dashed line represents the linear tendency along with their correlation coefficients. (For interpretation of the references to color in this figure legend, the reader is referred to the Web version of this article.)

calculation of K_{1C}: Eq. (4) for Palmqvist cracks was only used for sample B, while Eq. (5) for median cracks was employed for the other ceramics. The values of K_{1C} are reported in Table 4. Between the manufactured ceramics, the porous spinel A showed the highest toughness with 2.6 MPa$\sqrt{m}$, whereas the dense samples presented close or lower results: 1.6, 1.8, 2.5 and 1.9 MPa$\sqrt{m}$ respectively for samples B, C, D and E. Spinel fracture toughness values reported in the literature are quite scattered depending on the methods and the formulas used, or depending from the homogeneity of the microstructure [1,4,59,61,62].

- *Flexural strength*

Fig. 5 shows the 2-parameters Weibull distributions of the different grades of spinel obtained from the B3B tests. From this graph, the Weibull modulus was estimated as the slope of each curve (Table 4).

After a single pressureless sintering, the porous spinel A presented a Weibull modulus equal to 5.6. The application of a HIP treatment at 1800 °C influenced the distribution of defects, as the values decreased to 5.3 and 4.3 for samples B and C respectively. However, the sintering and HIP conditions for sample D led to a better homogenisation of the defects in the microstructure, as shown by its higher Weibull modulus (equal to 6.8). The same result has been observed for the commercial ceramic, presenting an even higher Weibull modulus of 7.2, indicating the most homogeneous repartition of the defects among the tested grades of ceramics.

With the aid of the graph in Fig. 5 and Eqs. (6)–(8), the average failure stress σ_{av} was obtained for each grade of spinel (Table 4). The porous ceramic A presented an average failure stress equal to 253 MPa. After the application of a post-treatment at 1800 °C, the value drastically decreased and reached 170 and 194 MPa for ceramics B and C respectively. The conditions applied for ceramic D did not impact as much this property, as a value equal to 242 MPa was obtained. However, by considering the standard deviation, all the sintered ceramics globally showed similar values. In the case of the commercial spinel, its flexural strength greatly outperformed the sintered samples with a result of 556 MPa. The comparison of these results with the literature is delicate, as no results of B3B tests for $MgAl_2O_4$ are reported, as far as the authors know. Studies showed diverse values of bending strength depending on the method used and the grain size of the ceramics. Results can reach 70–300 MPa with 3-point flexion test [22,48,58]. With the ring-on-ring method, values equal to 77 and 169 MPa were respectively reported for a coarse and fine grained spinel microstructures [59]. Strength of 470 MPa was even outlined for nanostructured spinel [61]. From the commercial data of CeramTec, the PERLUCOR spinel presented a bending strength of 300–350 MPa, with no indication of the methodology [63].

Thereafter, ceramic fractures were analysed by SEM. As shown in Fig. 3, the samples presented different fracture modes depending on the grain size and their distribution. Samples A and D showed both modes where intergranular fracture was predominant, whereas transgranular mode was mainly observed on samples B and C. In the case of the commercial spinel E, both modes were found as well and attributed to the bimodal grain size distribution. The transition from intergranular to transgranular mode was already reported in the literature when grain size increases [62,64,65].

3.5. Ballistic performance

Photos taken from the high-speed camera showcased some ballistic tests from this study (Fig. 6). The series of photos taken at different times in Fig. 6A and B illustrate a multilayer without a spinel layer,

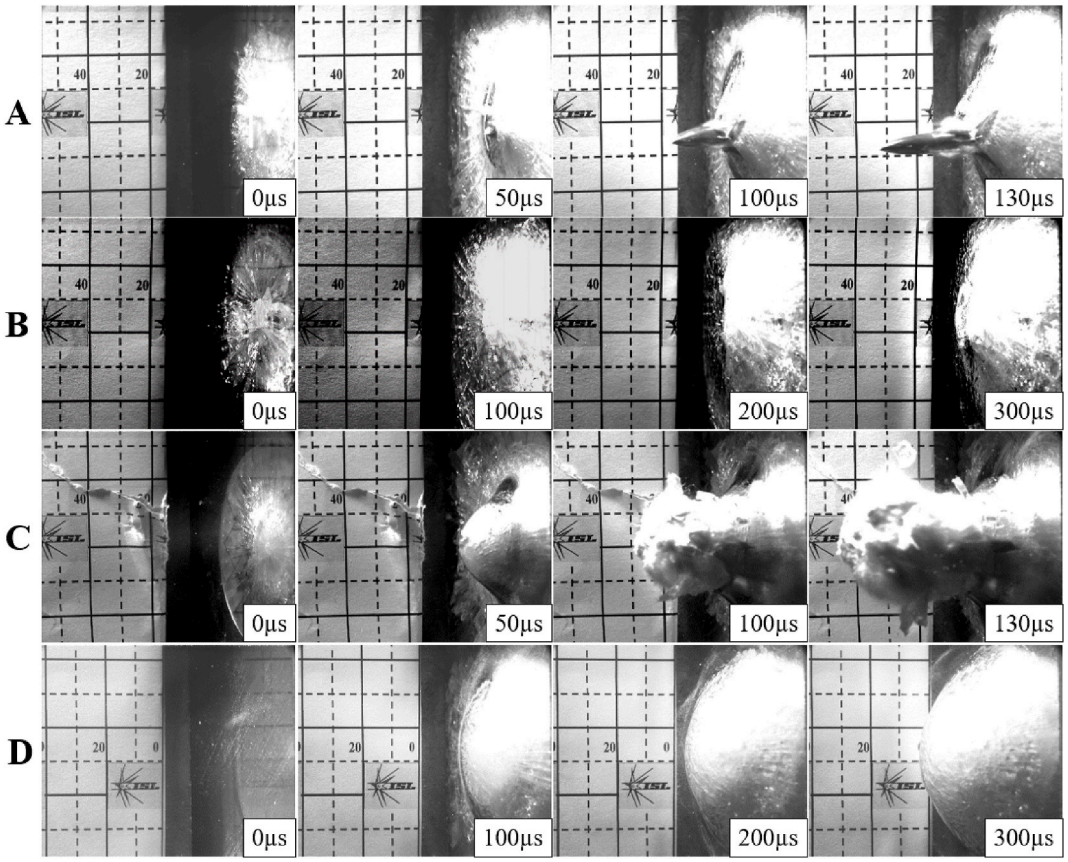

Fig. 6. Photos of perforated and non-perforated multilayers from the high-speed camera. (A) and (B) present the rear face of a negative and a positive tests on an assembly without ceramic, while (C) and (D) showcase tests made on a multilayer with a spinel layer as the front face. The time lapses are outlined on each picture.

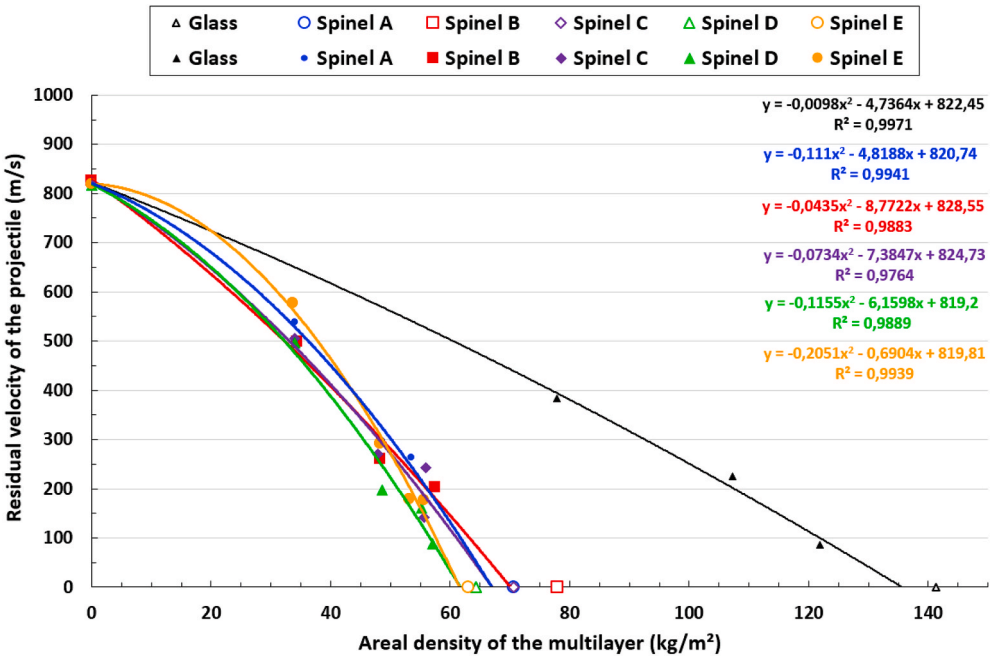

Fig. 7. Residual velocity of the projectile as function of the areal density of the multilayer. The lines represent the tendency curves for each configuration obtained from each shot (solid symbols). The equations and the correlation coefficients are mentioned for each curve. The empty symbols represent the tests were the multilayer withstood the shot. (For interpretation of the references to color in this figure legend, the reader is referred to the Web version of this article.)

Table 5
Areal density, thickness and LAD of the non-perforated multilayers.

Characteristics of the non-perforated multilayer	Glass	A	B	C	D	E
Areal density (kg/m^2)	141.4	70.6	78	70.6	64.4	63
Thickness (mm)	60	29.1	32.1	29.1	26.4	26
Change in thickness (%)		- 52	- 47	- 52	- 56	- 57
Limit Areal Density (LAD) (kg/m^2)	135.7	64.6	70.1	67	61.7	61.6
Change in areal density (%)		- 52	- 48	- 51	- 55	- 55

corresponding to tests #1 and #4 in *glass* configuration (Table 2). When the glass thickness was equal to 30 mm (test #1), the projectile perforated the different layers in a time lapse of 130μs. In the case of test #4 with 54 mm of glass, the multilayer withstood the shot, as seen by the deformation of the backing after 300μs (Fig. 6B). Fig. 6C and D presents a negative and a positive tests obtained on one configuration with a spinel as the front face (tests #1 and #4 with spinel B in Table 2). With a total thickness equal to 14.2 mm (test #1), the assembly was ineffective to stop the projectile, as it completely pierced the layers after 100μs (Fig. 6C). In the case of test #4, a multilayer of 32.1 mm was successful to stop the projectile. For complementary comparison, test #1 in *glass* configuration (Fig. 6A) and test #4 with the spinel B (Fig. 6D) showcased multilayers with similar AD (78 kg/m^2). Hence, it illustrates the advantage of a ceramic layer to decrease the thickness of a multilayer and its efficiency against projectiles.

On the basis of all the negative tests (*i.e.* with complete perforation) presented in Table 2, the residual velocity of the projectile as function of the areal density of the multilayer can be represented (Fig. 7). A second degree polynomial equation was used to obtain the general tendency for each configuration. By looking at the intersection of the curve with the x-axis, the Limit Areal Density (LAD) was obtained, which corresponds to the limit beyond which no perforation will be observed. Table 5 reports the areal density and the thickness of the positive tests (*i.e.* without perforation) for each configuration, represented by the empty symbols (Fig. 7), as well as the estimated LAD. The black curve in Fig. 7 is associated with the protection tested without a ceramic layer, labelled *glass*. As the AD increased, the residual velocity of the projectile decreased. By using only glass, a thickness of 60 mm in total (56 mm of glass and 4 mm of polycarbonate) was needed to stop the projectile, corresponding to an AD of 141.4 kg/m^2 (empty black symbol). As shown in Fig. 7, the LAD was lower than the experimental shot: a multilayer of 135.7 kg/m^2 should be efficient enough to resist the impact in these conditions (Table 5).

As it can be noticed, the addition of any type of spinel as the front face greatly reduced the AD. Although the results were quite close between the different grades, some ceramics stand out. Looking at the shots made for equivalent AD, at 34 kg/m^2 or 48 kg/m^2 (tests #1 and #2), the lowest V_r were obtained with samples B and D (red and green) as front face. On the other hand, the porous sample A (blue) seemed to be the less efficient ceramic of all the fabricated samples, as the measured residual velocities were the highest. In the case of sample C, intermediate results were obtained.

Sample D clearly demonstrated its efficiency compared to the others with the lightest non-perforated multilayer (empty green symbol), corresponding to 64.4 kg/m^2 and equivalent to 26.4 mm in total thickness, whereas the assembly with sample B (empty red symbol) weighted the most with 78 kg/m^2 (32.1 mm). The multilayers with samples A and C showed identical results with AD of 70.6 kg/m^2 for a thickness equal to 29.1 mm. Finally, the commercial sample E presented similar protective efficiency than our ceramic D: the multilayer including this spinel needed to be only 26 mm thick (63 kg/m^2) to be able to stop the projectile.

The estimation of the LAD reached the same conclusion as the experimental. The use of samples D and E allowed the best decrease of

AD of a transparent multilayer by 56–57% of reduction in thickness compared to the *glass* configuration. The opaque sample A, surprisingly, came next in term of efficiency. Finally, there were samples C and B, with AD above 67 kg/m^2, which corresponded to a decrease of 48–51% in AD compared to the multilayer without spinel.

4. Discussion

4.1. Influence of the microstructure on the optical properties

The optical quality of the sintered ceramics was mostly related to the presence of porosity, as no secondary phases or impurities were observed on the SEM images (Fig. 3). Sample A was the only spinel presenting porosity. The absence of transmission between 0.3 and 2 μm was mainly linked to the quantity and the size of the pores. As their diameters were close to the wavelengths of the visible range, the optical quality dropped significantly. The non-transparency in the infrared was caused by the numerous pores in the microstructure, leading to light scattering.

Very high transmissions were obtained for samples B, C and D after HIP due to the absence of pores of the same order of magnitude as the wavelengths of the visible. Microstructures without defects were obtained from different parameters of pressureless sintering and HIP, leading to high transmission in the visible and the infrared ranges, which were found to be comparable to the commercial. No influence of the grain size distribution was observed on the optical quality, this observation being consistent with the isotropic cubic structure of $MgAl_2O_4$.

4.2. Influence of the microstructure on the mechanical properties

Pressureless sintered ceramic A showed the lowest values of Knoop hardness and HK ∞ due to the presence of porosity, as described in other studies [66–69]. The application of a HIP treatment allowed an elimination of defects and an increase of density, thus an improvement of the hardness, as shown by the results on transparent ceramics (Fig. 4). This is in agreement with the literature, as it is known that hardness is improved when the grain size is decreased according to the Hall-Petch relation [16,57,61,70]. Sample D presented a microstructure with fine grains, leading to high hardness values. The presence of a majority of small grains and an overall low average grain size for sample E (visible in Fig. 3) explained the elevated values for this ceramic. Due to their coarse microstructures and heterogeneous grain size distributions, samples B and C showed lower values than samples D and E.

As reported in Table 4, elastic moduli of the different ceramics were of the same order of magnitude despite the various microstructures. Works from the state of the art indicate a negative impact of the porosity on the modulus: the value decreased when the density of the ceramic decreased [71–74]. In the presented work, sample A was the only porous ceramic. However, the lowest value was obtained with sample C, a dense and transparent spinel. Thus, it could be suggested that the poor level of porosity of sample A did not impact the measurements of transversal and longitudinal waves velocities as we could have expected. Although, from these results, no influence of the grain size and homogeneity was highlighted on this mechanical property. This is consistent with the conclusions of Sokol et al. [58] and Rothman et al. [60] who reported an independence of the elastic modulus from the grain size.

From the fracture toughness results of this study, a tendency can be observed: heterogeneous and large microstructure led to low value, as demonstrated by samples B and C, whereas homogeneous and fine microstructure induced higher toughness (samples A and D). The bimodal grain size distribution of sample E gave then an intermediary result due to its low grain size. These observations are in adequacy with the work of Tokariev et al. [59], where Niihara and Anstis formulas were used. However, the comparison with the literature is more complex, as this mechanical property relies on the ceramic, the microstructure, the method used and the model employed. For cubic materials, the statement made by Rice [64] showcased no grain size dependence of toughness, or slight decrease at finer, or larger grain sizes, or both, despite the difference in test methods. In the case of the dependence of the porosity, our results indicated no drawback to the presence of 3% of pores, as the porous sample A presented the highest value of fracture toughness. As pointed out by Rice, a low percentage of porosity (1–4%) is not as deleterious as suspected. A porous ceramic may show higher K_{1C} compared to denser samples [64,75].

The analysis of the Weibull modulus indicated a similar tendency compared to the other characterised properties: a fine and homogeneous microstructure gave favourable results with high moduli (samples A and D), whereas coarsening and heterogeneous grain size distributions resulted in more deleterious outcomes, which indicated disparate spread of the defects in the ceramic (samples B and C). The commercial ceramic E presented the highest Weibull modulus, which proved a low dispersion of the failure stresses. The porosity was not detrimental for this property, as sample C showed the lowest result instead of sample A. However, it must be reminded that a lower number of processed samples was tested compared to the commercial reference, this could influence the statistical study and, as a consequence, the Weibull moduli and failure stresses results.

Between the sintered ceramics, samples A and D presented higher mean failure stress compared to samples B and C. The homogeneous state of the microstructure and the low grain size looked, again, more advantageous to induce better mechanical properties. However, despite having a bimodal microstructure as samples B and C, sample E presented an exceptionally high failure stress. This could first be linked to the method used (B3B), as the comparison made by Danzer et al. [76] between B3B and bending test showed higher results of failure stress with B3B on different materials. Additionally, this result could also be attributed to the heterogeneity of sample E itself. Indeed, the paper of Jiang et al. [65] presented higher static compression strength on bimodal grain structure of $MgAl_2O_4$ compared to an monomodal ceramic. This was correlated to the fine grained region in the inhomogeneous structure, which creates more tortuous crack propagation paths. The better flexural stress of sample E in comparison with the other heterogeneous samples (B and C) can be explained by its lower average grain size (Table 3). In our study, a majority of fine grains favoured intergranular fracture mode, as demonstrated by samples A, D and E, resulting in higher K_{1C} [65,77,78]. Nonetheless, in the case of spinel ceramics, it has already been reported that both modes of fracture can be observed for small grains and intergranular mode for larger grains [59], this was not the case in this work.

4.3. Influence of the mechanical properties on the ballistic performance

The correlation between mechanical properties and ballistic performance is complex, as a single characteristic cannot predict the outcome and the efficiency of the material against a threat, and other parameters, such as the type of backing and projectile, the impact velocity or the thickness of the ceramic, can affect the results as well [7]. During a ballistic event, successive phenomena occur and different properties of the ceramic are involved. First, the projectile tip comes in contact with the front layer, where it is stopped during few microseconds (this event is called “dwell”), causing a loss of velocity and the nose of the AP core to break or erode, and the apparition of fractures in the ceramic. Then, the projectile breaks due to tensile stress released from the armour surface, whereas the ceramic and the backing plates are deformed. Finally, large fractures propagate through the ceramic plate, while the remaining AP core penetrates the ceramic fragments and the backing layer. According to several papers, during the dwell time, the Young modulus of the ceramic has the most important contribution, whereas the hardness of the fragments has an important role during penetration [77,79–81]. However, in order to compare different samples, a combination of properties should be considered and analysed: density/porosity, hardness, fracture toughness, fracture mode, Young modulus and mechanical

strength [7,77,78].

The presence of porosity in the ceramic was mentioned as beneficial in the work of Fakolujo et al. [82]. A homogeneous distribution of small size pores can retard the fracture initiation, then improving the residual strength of the material. This factor partially explains the better results of the porous sample A compared to several dense samples (including B and C).

Hardness is mostly cited as one of the principal properties to consider in ballistic [7,77,80,83]. A ceramic with high hardness will resist the penetration and blunt the projectile. Some studies indicate that hardness is directly linked to ballistic performances, whereas others suggest that the ceramic hardness only needs to be higher than the projectiles. In the presented work, the determination of the load-independent $HK\infty$ did not completely foresee the ballistic results. Samples D and E presented the highest $HK\infty$ and the best ballistic performances. Sample A was characterised by the lowest hardness but its ballistic efficiency was higher than samples B and C.

Results of K_{1C} alone cannot anticipate the outcome in ballistic as well. Between the sintered ceramics, samples A and D presented the highest results and efficiencies against a projectile, compared to samples B and C. However, the commercial spinel E was as efficient as samples A and D with a lower K_{1C} value. Dresch et al. [78] precise that a fracture toughness should be as high as possible in order to improve the ability of the material to resist various impacts. Flinders et al. [84] showed instead that a high level of K_{1C} will not mandatorily result in better ballistic performance.

The elastic modulus of the ceramic was pointed out as one of the main properties influencing the dwell time at the impact and the mode of fragmentation [7,78,80]. High value can prolong the interaction of the projectile with the ceramic surface, which is beneficial for ballistic performance, and cause less cracks, wider crack spacing and larger fragments [78]. However, in some circumstances, where the contribution of dwell-phase interactions to the ballistic result is small, this theory is not respected and the ceramic, even if it presents a high E, may not exhibit the best ballistic performances [80]. In this work, sample B showed the highest value but the worst ballistic result. Nonetheless, no substantial differences in the Young modulus values of our ceramics were found, hence no correlation can be made from these results.

Kumar et al. [8] indicated that ballistic performance should be correlated with the strength of the material under tensile, compressive, shear, and bending modes, rather than a single strength value, as the ceramic undergoes many solicitations at the impact. Although Krell and Strassburger [80] did not add the material strength in their hierarchy (established for small calibre projectiles at impact velocities up to 1000 m/s), it should be considered nonetheless when different ceramics are compared. In the article of Dresch et al. [78], tensile strength is cited as one of the parameters that can act on the performance of the material, notably in the ability to withstand multiple impacts. In this work, flexural strength (instead of tensile strength) was determined and followed the ballistic results: samples B and C with the lowest σ_{av} did not demonstrate the best efficiency in comparison with samples A and D. However, the commercial spinel value stood out between all the tested samples but showed close ballistic results to sample D. This observation may suggest that flexure strength had a limited influence on the ballistic outcome in the tested conditions described in this article.

Finally, the fracture mode also played a role in the efficiency against an AP projectile. Sample showing a majority of intergranular fracture is advantageous, as cracks will follow a more sinuous path through the grain boundaries, which will require more energy to create a larger fracture surface [77]. This aspect was demonstrated by samples A, D and E.

In closing, as a small number of samples of each grade were characterised in this work, the previous discussions are subject to debate and have to be confirmed with supplementary tests.

5. Conclusion

This work dealt with the characterisation and the ballistic evaluation of $MgAl_2O_4$ spinel ceramics manufactured by pressureless sintering and hot isostatic pressing from a pure commercial powder without using any additives. By varying sintering and HIP conditions, four samples exhibiting different final microstructures were produced. The influence of the grain size and their distribution on the mechanical properties and the ballistic performances was discussed. In addition to the processed samples, a commercial transparent ceramic purchased from CeramTec was used as reference.

A thorough analysis was firstly performed in order to highlight the differences in the microstructures of the ceramics. A correlation between microstructural properties and mechanical properties was undertaken. Among the manufactured ceramics, a highly transparent ceramic exhibiting remarkable in-line transmission (77–83%) in the visible range was developed. Higher values of Knoop hardness, fracture toughness and flexural strength were obtained for the ceramics with homogeneous and fine-grained microstructures, compared to spinel with large and heterogeneous grain size distributions. The ceramic with 3% of porosity presented better properties in term of toughness and flexural strength compared to the dense samples with coarse grains. The commercial ceramic presenting a bimodal grain distribution with a large proportion of fine grains showed a good combination of properties, comparable to the processed ceramics with fine grains.

Secondly, the ballistic performances of the ceramics were tested, where the spinel samples were used as the strike face of a transparent assembly made of glass and polycarbonate. By varying the glass thicknesses, the limit areal density was determined for each of the considered ceramic. The presence of a 4 mm-fabricated ceramic layer led to considerable reductions of 48–55% and 47–57% respectively in weight and thickness, compared to a glass protection. The commercial reference was tested in the same configuration and a similar ballistic performances as the most efficient manufactured ceramic, presenting a fine and narrow grain size distribution, was obtained leading to a 55% weight gain and 57% thickness reduction.

These first results based on a limited number of samples allowed to highlight the benefit of a microstructure, non- or homogeneous, with a majority of small grains in order to obtain better mechanical properties, hence higher ballistic efficiency compared to $MgAl_2O_4$ spinel with large grains. Nonetheless, supplementary samples and characterisations are necessary to improve the statistic and determine better correlation between mechanical properties and ballistic outcome.

Declaration of competing interest

The authors declare that they have no known competing financial interests or personal relationships that could have appeared to influence the work reported in this paper.

Acknowledgements

C. Gajdowski is now working as researcher in the Belgium Ceramic Research Centre (Mons, Belgium). The authors thank the Direction Générale de l'Armement (DGA, France) for funding this research through the Ph.D. grant #2014600054 awarded to C. Gajdowski.

References

[1] M. Grujicic, W.C. Bell, B. Pandurangan, Design and material selection guidelines and strategies for transparent armor systems, Mater. Des. 34 (2012) 808–819.
[2] P.J. Patel, G.A. Gilde, P.G. Dehmer, J.W. McCauley, Transparent armor, Adv. Mater. Process. 4 (3) (2000).
[3] W. Kim, et al., Overview of transparent optical ceramics for high-energy lasers at NRL, Appl. Opt. 54 (31) (2015) F210.
[4] R. Johnson, P. Biswas, P. Ramavath, R.S. Kumar, G. Padmanabham, Transparent polycrystalline ceramics: an overview, Trans. Indian Ceram. Soc. 71 (2) (2012) 73–85.
[5] T. Benitez, S.Y. Gómez, A.P.N. de Oliveira, N. Travitzky, D. Hotza, Transparent ceramic and glass-ceramic materials for armor applications, Ceram. Int. 43 (16) (2017) 13031–13046.
[6] A. Krell, T. Hutzler, J. Klimke, Defect strategies for an improved optical quality of transparent ceramics, Opt. Mater. 38 (2014) 61–74.
[7] A. Krell, E. Strassburger, Order of influences on the ballistic resistance of armor ceramics and single crystals, Mater. Sci. Eng., A 597 (2014) 422–430.
[8] R.S. Kumar, P. Biswas, R. Johnson, Y.R. Mahajan, Transparent ceramics for ballistic armor applications, in: Handbook of Advanced Ceramics and Composites, Springer International Publishing, 2020.
[9] A. Krell, J. Klimke, T. Hutzler, Advanced spinel and sub-μm Al2O3 for transparent armour applications, J. Eur. Ceram. Soc. 29 (2) (2009) 275–281.
[10] E. Strassburger, Ballistic testing of transparent armour ceramics, J. Eur. Ceram. Soc. 29 (2) (2009) 267–273.
[11] A. Goldstein, A. Krell, Transparent ceramics at 50: progress made and further prospects, J. Am. Ceram. Soc. 99 (10) (2016) 3173–3197.
[12] R. Klement, S. Rolc, R. Mikulikova, J. Krestan, Transparent armour materials, J. Eur. Ceram. Soc. 28 (5) (2008) 1091–1095.
[13] A. Krell, E. Strassburger, T. Hutzler, J. Klimke, Single and polycrystalline transparent ceramic armor with different crystal structure, J. Am. Ceram. Soc. 96 (9) (2013) 2718–2721.
[14] N. Hansen, Hall–Petch relation and boundary strengthening, Scripta Mater 51 (8) (2004) 801–806.
[15] C.S. Pande, K.P. Cooper, Nanomechanics of Hall-Petch relationship in nanocrystalline materials, Prog. Mater. Sci. 54 (2009) 689–706.
[16] M. Sokol, M. Halabi, S. Kalabukhov, N. Frage, Nano-structured MgAl2O4 spinel consolidated by high pressure spark plasma sintering (HPSPS), J. Eur. Ceram. Soc. 37 (2) (2017) 755–762.
[17] M. Azizi-Malekabadi, R. Sarraf-Mamoory, Devising a novel method of producing high transparent magnesium aluminate spinel (MgAl2O4) ceramics body using synthesized LiF nanopowder and spark plasma sintering, Mater. Chem. Phys. 250 (2020) 123035.
[18] S. Cohen, B. Ratzker, M. Sokol, S. Kalabukhov, N. Frage, Polycrystalline transparent magnesium aluminate spinel processed by a combination of spark plasma sintering (SPS) and hot isostatic pressing (HIP), J. Eur. Ceram. Soc. 38 (15) (2018) 5153–5159.
[19] L.-L. Zhu, et al., Fabrication of transparent MgAl2O4 from commercial nanopowders by hot-pressing without sintering additive, Mater. Lett. 219 (2018) 8–11.
[20] K. Maca, M. Trunec, R. Chmelik, Processing and properties of fine-grained transparent MgAl2O4 ceramics, Ceramics 51 (2) (2006) 94–97.
[21] G. Bernard-Granger, N. Benameur, C. Guizard, M. Nygren, Influence of graphite contamination on the optical properties of transparent spinel obtained by spark plasma sintering, Scripta Mater 60 (3) (2009) 164–167.
[22] P. Ramavath, et al., Optical and mechanical properties of compaction and slip cast processed transparent polycrystalline spinel ceramics, Ceram. Int. 40 (4) (2014) 5575–5581.
[23] G. Bonnefont, G. Fantozzi, S. Trombert, L. Bonneau, Fine-grained transparent MgAl2O4 spinel obtained by spark plasma sintering of commercially available nanopowders, Ceram. Int. 38 (1) (2012) 131–140.
[24] A. Goldstein, A. Goldenberg, M. Hefetz, Transparent polycrystalline MgAl2O4 spinel with submicron grains, by low temperature sintering, J. Ceram. Soc. Jpn. 117 (1371) (2009) 1281–1283.
[25] K. Morita, B.-N. Kim, K. Hiraga, H. Yoshida, Fabrication of transparent MgAl2O4 spinel polycrystal by spark plasma sintering processing, Scripta Mater 58 (12) (2008) 1114–1117.
[26] J.-M. Kim, H.-N. Kim, Y.-J. Park, J.-W. Ko, J.-W. Lee, H.-D. Kim, Fabrication of transparent MgAl2O4 spinel through homogenous green compaction by microfluidization and slip casting, Ceram. Int. 41 (10) (2015) 13354–13360.
[27] M.F. Zawrah, H. Hamaad, S. Meky, Synthesis and characterization of nano MgAl2O4 spinel by the co-precipitated method, Ceram. Int. 33 (6) (2007) 969–978.
[28] M. Suarez, V. Rocha, A. Fernandez, J.L. Menendez, R. Torrecillas, Synthesis and processing of spinel powders for transparent ceramics, Ceram. Int. 40 (3) (2014) 4065–4069.
[29] G. Li, Z. Sun, C. Chen, X. Cui, R. Ren, Synthesis of nanocrystalline MgAl2O4 spinel powders by a novel chemical method, Mater. Lett. 61 (17) (2007) 3585–3588.
[30] L. Esposito, A. Piancastelli, P. Miceli, S. Martelli, A thermodynamic approach to obtaining transparent spinel (MgAl2O4) by hot pressing, J. Eur. Ceram. Soc. 35 (2) (2015) 651–661.
[31] S. Meir, S. Kalabukhov, N. Froumin, M.P. Dariel, N. Frage, Synthesis and densification of transparent magnesium aluminate spinel by SPS processing, J. Am. Ceram. Soc. 92 (2) (2009) 358–364.
[32] I. Ganesh, G. Jaganatha Reddy, G. Sundararajan, S.M. Olhero, P.M.C. Torres, J.M. F. Ferreira, Influence of processing route on microstructure and mechanical properties of MgAl2O4 spinel, Ceram. Int. 36 (2) (2010) 473–482.
[33] A.F. Dericioglu, Y. Kagawa, Effect of grain boundary microcracking on the light transmittance of sintered transparent MgAl2O4, J. Eur. Ceram. Soc. 23 (6) (2003) 951–959.
[34] I.E. Reimanis, R.L. Cook, A. DiGiovanni, Transparent Spinel Fabricated from Novel Powders: Synthesis, Microstructure and Optical Properties, SPIE, 2004.
[35] K. Waetzig, T. Hutzler, Highest UV–vis transparency of MgAl2O4 spinel ceramics prepared by hot pressing with LiF, J. Eur. Ceram. Soc. 37 (5) (2017) 2259–2263.
[36] G. Gilde, P. Patel, P. Patterson, D. Blodgett, D. Duncan, D. Hahn, Evaluation of hot pressing and hot isostastic pressing parameters on the optical properties of spinel, J. Am. Ceram. Soc. 88 (10) (2005) 2747–2751.
[37] S. Benaissa, M. Hamidouche, M. Kolli, G. Bonnefont, G. Fantozzi, Characterization of nanostructured MgAl2O4 ceramics fabricated by spark plasma sintering, Ceram. Int. 42 (7) (2016) 8839–8846.
[38] P. Fu, W. Lu, W. Lei, Y. Xu, X. Wang, J. Wu, Transparent polycrystalline MgAl2O4 ceramic fabricated by spark plasma sintering: microwave dielectric and optical properties, Ceram. Int. 39 (3) (2013) 2481–2487.
[39] K. Morita, B.-N. Kim, H. Yoshida, K. Hiraga, Y. Sakka, Assessment of carbon contamination in MgAl2O4 spinel during spark-plasma-sintering (SPS) processing, J. Ceram. Soc. Jpn. 123 (1442) (2015) 983–988.
[40] K. Morita, B.-N. Kim, H. Yoshida, K. Hiraga, Y. Sakka, Distribution of carbon contamination in MgAl2O4 spinel occurring during spark-plasma-sintering (SPS) processing: I - effect of heating rate and post-annealing, J. Eur. Ceram. Soc. 38 (6) (2018) 2588–2595.
[41] K. Rozenburg, I.E. Reimanis, H.-J. Kleebe, R.L. Cook, Sintering kinetics of a MgAl2O4 spinel doped with LiF, J. Am. Ceram. Soc. 91 (2) (2008) 444–450.
[42] K. Tsukuma, Transparent MgAl2O4 spinel ceramics produced by HIP post-sintering, J. Ceram. Soc. Jpn. 114 (10) (2006) 802–806.
[43] M. Rubat du Merac, I.E. Reimanis, C. Smith, H.-J. Kleebe, M.M. Müller, Effect of impurities and LiF additive in hot-pressed transparent magnesium aluminate spinel, Int. J. Appl. Ceram. Technol. 10 (2013) E33–E48.
[44] A.C. Sutorik, G. Gilde, C. Cooper, J. Wright, C. Hilton, The effect of varied amounts of LiF sintering aid on the transparency of alumina rich spinel ceramic with the composition MgO · 1.5 Al2O3, J. Am. Ceram. Soc. 95 (6) (2012) 1807–1810.
[45] I. Reimanis, H.-J. Kleebe, A review on the sintering and microstructure development of transparent spinel ($MgAl_2O_4$), J. Am. Ceram. Soc. 92 (7) (2009) 1472–1480.
[46] A. Katz, et al., Role of LiF additive on spark plasma sintered transparent YAG ceramics, Ceram. Int. 43 (17) (2017) 15626–15634.
[47] A. Krell, T. Hutzler, J. Klimke, A. Potthoff, Fine-grained transparent spinel windows by the processing of different nanopowders, J. Am. Ceram. Soc. 93 (9) (2010) 2656–2666.
[48] Q. Liu, et al., Microstructure and properties of MgAl2O4 transparent ceramics fabricated by hot isostatic pressing, Opt. Mater. 104 (2020) 109938.
[49] A. Shafeiey, M.H. Enayati, A. Al-Haji, The effect of slip casting parameters on the green density of MgAl2O4 spinel, Ceram. Int. 43 (8) (2017) 6069–6074.
[50] J.W. McCauley, P. Patel, Evaluation of IKTS Transparent Polycrystalline Magnesium Aluminate Spinel (MgAl2O4) for Armor and Infrared Dome/Window Applications, Army Research Laboratory, 2013.
[51] C. Gajdowski, et al., Influence of post-HIP temperature on microstructural and optical properties of pure MgAl2O4 spinel: from opaque to transparent ceramics, J. Eur. Ceram. Soc. 37 (2017) 5347–5351.
[52] P.J. Patel, J.J. Swab, M. Staley, G.D. Quinn, Indentation Size Effect (ISE) of Transparent AlON and MgAl2O4, ARL, 2006.
[53] A. Carpinteri, S. Puzzi, A fractal approach to indentation size effect, Eng. Fract. Mech. 73 (15) (2006) 2110–2122.
[54] K. Niihara, A fracture mechanics analysis of indentation-induced Palmqvist crack in ceramics, J. Mater. Sci. Lett. 2 (5) (1983) 221–223.
[55] A. Börger, P. Supancic, R. Danzer, The ball on three balls test for strength testing of brittle discs: stress distribution in the disc, J. Eur. Ceram. Soc. 22 (9) (2002) 1425–1436.
[56] A. Börger, P. Supancic, R. Danzer, The ball on three balls test for strength testing of brittle discs: Part II: analysis of possible errors in the strength determination, J. Eur. Ceram. Soc. 24 (10) (2004) 2917–2928.
[57] A. Krell, A. Bales, Grain size-dependent hardness of transparent magnesium aluminate spinel, Int. J. Appl. Ceram. Technol. 8 (5) (2011) 1108–1114.
[58] M. Sokol, S. Kalabukhov, R. Shneck, E. Zaretsky, N. Frage, Effect of grain size on the static and dynamic mechanical properties of magnesium aluminate spinel (MgAl2O4), J. Eur. Ceram. Soc. 37 (10) (2017) 3417–3424.
[59] O. Tokariev, L. Schnetter, T. Beck, J. Malzbender, Grain size effect on the mechanical properties of transparent spinel ceramics, J. Eur. Ceram. Soc. 33 (4) (2013) 749–757.
[60] A. Rothman, S. Kalabukhov, N. Sverdlov, M.P. Dariel, N. Frage, The effect of grain size on the mechanical and optical properties of Spark Plasma Sintering-processed magnesium aluminate spinel MgAl2O4, Int. J. Appl. Ceram. Technol. 11 (1) (2014) 146–153.
[61] T. Mroz, L.M. Goldman, A.D. Gledhill, D. Li, N.P. Padture, Nanostructured, infrared-transparent magnesium-aluminate spinel with superior mechanical properties, Int. J. Appl. Ceram. Technol. 9 (1) (2012) 83–90.
[62] B. Mussler, M.V. Swain, N. Claussen, Dependence of fracture toughness of alumina on grain size and test technique, J. Am. Ceram. Soc. 65 (11) (1982) 566–572.
[63] CeramTec, 'THe Innovative Material for New Dimensions - PERLUCOR Transparent Ceramics'.
[64] R. Rice, Mechanical Properties of Ceramics and Composites: Grain and Particle Effects, CRC Press, 2000.
[65] W. Jiang, X. Cheng, Z. Xiong, T. Ali, H. Cai, J. Zhang, Bimodal grain structure effect on the static and dynamic mechanical properties of transparent polycrystalline

magnesium aluminate (spinel), Ceram. Int. 45 (16) (2019) 20362–20367, https://doi.org/10.1016/j.ceramint.2019.07.010.
[66] A.B. Hadzley, T. Norfauzi, U.A.A. Umar, A.A. Afuza, M.M. Faiz, M.F. Naim, Effect of sintering temperature on density, hardness and tool wear for alumina-zirconia cutting tool, J. Mech. Eng. Sci. 13 (1) (2019) 4648–4660.
[67] G. Mata-Osoro, J.S. Moya, C. Pecharroman, Transparent alumina by vacuum sintering, J. Eur. Ceram. Soc. 32 (11) (2012) 2925–2933.
[68] D. Lipusz, Á. Isztli, L.A. Gömze, Influence of sintering time on properties of alumina-based ceramic composite, Inside MS 812 (2015) 143–147.
[69] B.M. Moshtaghioun, D. Gomez-Garcia, A. Dominguez-Rodriguez, Richard I. Todd, Grain size dependence of hardness and fracture toughness in pure near fully-dense boron carbide ceramics, J. Eur. Ceram. Soc. 36 (7) (2016) 1829–1834.
[70] M. Sokol, M. Halabi, Y. Mordekovitz, S. Kalabukhov, S. Hayun, N. Frage, An inverse Hall-Petch relation in nanocrystalline MgAl2O4 spinel consolidated by high pressure spark plasma sintering (HPSPS), Scripta Mater 139 (2017) 159–161.
[71] M. Asmani, C. Kermel, A. Leriche, M. Ourak, Influence of porosity on Young's modulus and Poisson's ratio in alumina ceramics, J. Eur. Ceram. Soc. 21 (8) (2001) 1081–1086.
[72] A. Tricoteaux, et al., Influence of porosity on the mechanical properties of microporous β-TCP bioceramics by usual and instrumented Vickers microindentation, J. Eur. Ceram. Soc. 31 (8) (2011) 1361–1369.
[73] A. Atkinson, P. Bastid, Q. Liu, Mechanical properties of magnesia-spinel composites, J. Am. Ceram. Soc. 90 (8) (2007) 2489–2496.
[74] A.R. Boccaccini, Z. Fan, A new approach for the Young's modulus-porosity correlation of ceramic materials, Ceram. Int. 23 (3) (1997) 239–245.
[75] R.W. Rice, Grain size and porosity dependence of ceramic fracture energy and toughness at 22°C, J. Mater. Sci. (1996).
[76] R. Danzer, W. Harrer, P. Supancic, T. Lube, Z. Wang, A. Börger, The ball on three balls test–Strength and failure analysis of different materials, J. Eur. Ceram. Soc. 27 (2–3) (2007) 1481–1485.
[77] P.G. Karandikar, G. Evans, S. Wong, M.K. Aghajanian, M. Sennett, A review of ceramics for armor applications, in: L.P. Franks (Ed.), Ceramic Engineering and Science Proceedings, John Wiley & Sons, Inc., 2008, pp. 163–175.
[78] A.B. Dresch, J. Venturini, S. Arcaro, O.R.K. Montedo, C.P. Bergmann, Ballistic ceramics and analysis of their mechanical properties for armour applications: a review, Ceram. Int. (2020).
[79] R.L. Woodward, W.A. Gooch, R.G. O'Donnell, W.J. Perciballi, B.J. Baxter, S. D. Pattie, A study of fragmentation in the ballistic impact of ceramics, Int. J. Appl. Ceram. Technol. 15 (5) (1994) 605–618.
[80] A. Krell, E. Strassburger, Hierarchy of key influences on the ballistic strength of opaque and transparent armor, in: Advances in Ceramic Armor III, 2008.
[81] C. Kaufmann, D. Cronin, M. Worswick, G. Pageau, A. Beth, Influence of material properties on the ballistic performance of ceramics for personal body armour, Shock Vib. 10 (1) (2003) 51–58.
[82] O. Fakolujo, A. Merati, M. Bielawski, M. Bolduc, M. Nganbe, Role of microstructural features in toughness improvement of zirconia toughened alumina, JMMCE (2016) 87–102, 04, no. 01.
[83] M.V. Demirbas, Microstructure-property Relationship in Silicon Carbide Armor Ceramics, Rutgers University, USA), 2008.
[84] M. Flinders, D. Ray, A. Anderson, R.A. Cutler, High-toughness silicon carbide as armor, J. Am. Ceram. Soc. 88 (8) (2005) 2217–2226.